Taylor & Francis
Taylor & Francis Group

Journal of Medical Engineering & Technology

Evaluating the Accuracy of 3D Printing and Finite Element Analysis in Transcatheter Aortic Valve Implantation: A Comparative Study Against Post-TAVI CT Imaging

Submission ID	251989119
Article Type	Research Article
Keywords	Keywords: Transcatheter aortic valve implantation, 3D Printing, finite-element analysis, transcatheter heart valves
Authors	fabrizio crascì, Stefano Cannata, caterina gandolfo, salvatore pasta

Evaluating the Accuracy of 3D Printing and Finite Element Analysis in Transcatheter Aortic Valve Implantation: A Comparative Study Against Post-TAVI CT Imaging

Fabrizio Crascì[1,2], Stefano Cannata[3], Caterina Gandolfo[3], Salvatore Pasta[1,2]

[1] Department of Engineering, Università degli Studi di Palermo, Viale delle Scienze Ed.8, Palermo, Italy

[2] Department of Research, IRCCS ISMETT via Tricomi, 5, Palermo, Italy

[3] Department for the Treatment and Study of Cardiothoracic Diseases and Cardiothoracic Transplantation, IRCCS-ISMETT (Istituto Mediterraneo per i Trapianti e Terapie ad alta Specializzazione), Palermo, Italy.

Word count: 4867

*Correspondence:
Corresponding author:
Salvatore Pasta, PhD
Professor of Bioengineering,
Department of Engineering
University of Palermo
office: +39 09123897277
email: salvatore.pasta@unipa.it

Abstract

Transcatheter aortic valve implantation (TAVI) has become the standard therapy for the treatment of aortic stenosis as a less invasive and equally effective treatment compared to surgical repair. While 3D printing and finite element analysis (FEA) have emerged as promising tools for pre-procedural planning, the reliability of these approaches in predicting post-TAVI device configuration remains uncertain. This study aims to assess the consistency and agreement of patient-specific FEA models and 3D-printing replicas in replicating implanted device geometry compared to post-TAVI computed-tomography (CT) imaging. Ten patients undergoing TAVI with the SAPIEN 3 Ultra (S3) device were analyzed using pre- and post-TAVI CT imaging. Patient-specific 3D-printed phantoms and FEA-based simulations were generated to evaluate stent deformation and anatomical conformity. Statistical analyses, including concordance correlation coefficient (CCC), intraclass correlation coefficient (ICC), and Bland-Altman plots, were employed to quantify the agreement between in-vitro, in-silico, and post-TAVI CT-derived diameter measurements. The FEA model exhibited better agreement with post-TAVI CT data (ICC Indiv = 0.614 and CCC = 0.479), whereas 3D printing showed lower correlation and higher measurement variability (ICC Loneway = 0.363 and CCC=0.165). While numerical simulations closely approximated device expansion at the annular level, both approaches exhibited deviations due to computational assumptions and material differences. This study underscores the potential of patient-specific computational and physical modeling for TAVI planning, with FEA demonstrating higher reliability in predicting implanted device geometry. However, methodological standardization and further validation are needed to enhance precision and optimize personalized TAVI procedures.

Keywords: Transcatheter aortic valve implantation; 3D Printing; finite-element analysis, transcatheter heart valves

1. Introduction

As life expectancy continues to rise, the prevalence of degenerative aortic stenosis of any calcification degree has increased to 40% of people aged 80 and beyond [1]. If the valvulopathy is not treated, the 5-year prognosis is poor after the initial medical imaging diagnosis [2]. In this context, transcatheter aortic valve implantation (TAVI) has evolved as the standard approach for treating aortic stenosis, with short-term outcomes comparable to surgical aortic valve replacement in the elderly [3].

3D printing and computer modeling applications have also seen technological advancements. Indeed, the combination of advanced imaging with either 3D printing or computer modeling has contributed to a substantial advancement in TAVI planning [4, 5]. Patient-specific 3D-printed models offer clinicians a physical envision of the anatomy, allowing them to visualize anatomical challenges and practice device deployment. Alkhouli et al [6] demonstrated the possibility of 3D printing patient replicas for TAVI planning, demonstrating that the manufacturing approach is both cost and time efficient. Schmauss et al. [7] showed how physical deployment of a TAVI-related device in a 3D printed phantom and adjustment of the implantation depth allowed for a more accurate evaluation of the device's interaction with coronary artery heights in complex anatomical structure. This technology also revealed data supporting a mechanistic relationship between post-TAVI risk of permanent pacemaker implantation and calcification of the left coronary cusps [8].

In contrast, computational modeling enables an accurate assessment of stent performance, including stress distribution, the likelihood of paravalvular leakage, and

contact with calcified areas [9]. Such insights can be very useful for tailoring the procedure for certain patients, lowering the likelihood of complications, and enhancing long-term outcomes. By comparing stent configurations across anatomical geometries, physicians may determine the best device for each patient and reduce the likelihood of prosthesis-patient mismatch [10]. Most notably, finite-element analysis (FEA) allows for simulation of "what-if" scenarios, such as different implantation depths or angulations, as illustrated by Finotello et al [11]. In a large cohort of 69 patients receiving both self- and balloon-expandable devices, Schults et al [12] displayed the importance of patient-specific simulations for accurate predictions of stent frame morphology at the implantation site and calcium displacement resulting from device deployment. As TAVI grows to include younger and redo-TAVI, the demand for precision planning tools based on FEAs is expected to rise, not only for showing the feasibility of complex TAVI procedures but also for offering insights for the next generation of transcatheter heart valves .

However, there is a lack of extensive comparative investigation to determine the reliability of both 3D printing and FEA as TAVI predictive tools. Standardization of numerical solver settings and boundary conditions in FEAs as well as materials and manufacturing process in 3D printing, is also weak. The purpose of this work was to implement a robust statistical analysis to measure the level of agreement in the device implanted configuration acquired from patient-specific TAVI simulations and in-vitro deployment on a 3D-printed replica against actual post-TAV imaging data. To ensure a rigorous comparison, the level of variability and agreement between in-silico and in-vitro predictions was determined using different statistical metrics and Blant-Altman graphs for visual comparison. The reliability of these technologies in comparison to actual post-TAVI computed tomography imaging is discussed.

2. Materials and Methods

2.1 Segmentation and 3D printing

This study included ten patients undergoing transcatheter aortic valve implantation (TAVI) for aortic valve stenosis with the balloon-expandable SAPIEN 3 Ultra (S3) device (Edwards Lifesciences, USA). Seven patients received treatment with the 23 mm S3 device, while three patients were treated with the 26 mm device. Imaging was performed utilizing electrocardiogram-gated CT (ECG-gated CT) with a 256-detector-row scanner (Somatom Force, Siemens, Germany) following the injection of a contrast agent. Cardiac synchronization allowed the assessment of ten image sets over the cardiac cycle, with a resolution of 512 × 512 pixels and a slice thickness of 0.625 mm. In this investigation, a second CT imaging was carried out thirty days after TAVI to assess the device diameters at the inflow, mid, and outflow levels of the device height.

After image acquisition, the aortic root geometry was segmented using early-diastolic pictures through Mimics medical analysis software (v21, Materialise, Belgium), as previously reported [13]. Threshold-based segmentation was employed for the aorta to define the grey intensity of the luminal wall, extending from the left ventricular outflow tract to the proximal ascending aorta. Native valve leaflets were produced using spline curves that delineated both the attachment to the sinuses and the free edge of the leaflets . Anatomical reference points were utilized to delineate the mid-height of the valve leaflets from the annulus. A surface network defining the valve leaflet was created using spline curves and anatomical locations in Rhinoceros software (v7, McNeel, USA). Calcifications were reconstructed by fully automated thresholding based on grey intensity values ranging

from 850 to 2145 Hounsfield units, followed by re-meshing using Delaunay triangulation. Each anatomical component was integrated in Rhinoceros to create the aortic root model and subsequently exported as a stereolithography file (STL) for rapid prototyping.

2.2 Phantom fabrication

Patient-specific anatomical models were printed using a LED-based photocuring 3D printer (Saturn, Elegoo, Shenzhen). A black flexible resin (Flexible-X, Liqcreate, Netherlands) was employed with mechanical specifications defined as a tensile strength of 2.4 MPa, an elongation at rupture of 120-160%, and a hardness of 55 HB. Optimization of parameter settings was required to fabricate the thin structure of valve leaflets. Specifically, layer height, exposure and thickness were varied to achieve a successful printing of valve leaflets without layer delamination or defects. The optimal key printing parameters comprised a layer height of 50 μm, a bottom layer count of 5, a speed of 60 mm/min, and an exposure duration of 10 seconds per layer to obtain optimal polymerization. Ten transition layer counts were employed to improve interlayer adhesion, with a rest period of 2 seconds established before and after lifting and retracting. Material support was restricted to the aorta wall and not utilized for the valve leaflets due to the risk of lacerating the delicate surface leaflets. The resulting thickness was 2 mm for the aortic wall and 0.5 mm for the valve leaflets. The post-processing included washing the models with isopropanol to eliminate excess resin, followed by UV curing for consistent polymerization. Support structures were meticulously extracted with precision instruments to maintain model integrity.

2.3 Deployment of S3 model in phantom

After each patient phantom was created, a replica of the S3 stent frame without biological valve leaflets, provided by Edwards Lifescience, was implanted in phatom models. The S3 was first crimped and then placed in the commander delivery mechanism with the folded balloon. The device was put in the annular position, with 1/3 of its length positioned below the annulus, as indicated by the manufacturer. The balloon was inflated with a syringe at the nominal fluid volume of 17 mL for the 23 mm device and 21 mL for the 26 mm device. Following in-vitro deployment, each phantom received CT scan imaging to assess the deformed shape of the stent frame using diameter measurements at the inflow, mid, and outflow device heights. The maximum and minimum device diameters were measured at each level, and the average value was utilized to compare with FEA predictions and actual clinical data.

2.4 In-silico TAVI simulation

A previously numerically verified and validated patient-specific model developed in accordance with the ASME V&V40 standard was used to simulate the TAVI procedure. Details about numerical verification [14], validation [15], and uncertainty quantification [13, 16] are provided elsewhere. In brief, each anatomical component was meshed utilizing grid refinements to assure a relative inaccuracy of less than 1.0% in the final stress distribution of the TAVI simulation. Numerical error analysis was established as well to decrease errors caused by solver settings (for example, damping and stable time increment)..

The aortic wall and native valve leaflets were modeled using Neo-Hookean material behavior, using constitutive parameters derived from an inverse analysis [17]. Peak-systolic CT scans were utilized to calculate the valve orifice area using perimetric measurement of the leaflet free edge and the aortic wall strain in relation to the diastolic

phase. By several simulations, the inverse analysis permitted the reduction of discrepancies in aortic wall strain and valve area between the pre-TAVI model and the CT-derived values. The resulting neo-Hookean material parameters were in the range of 0.25-1.24 MPa for the aortic wall and 0.68-2.5 MPa for the valve leaflets. The aortic wall model did not account for the pre-stress of the aortic wall, which presumably affects the TAVI simulation and wall stress distribution. Calcific plaques were modeled using a neo-Hookean material formulation with parameters C10=0.465 MPa and D1=0.109 MPa, as documented by Bosi and collaborators [18]. The stent frame of the medical device was modeled with structured hexahedral elements and cobalt-chromium material characteristics, employing a combination of isotropic elasticity and Johnson-Cook plasticity [17]. A second-order Ogden model was employed for the biological valve leaflets, while a neo-Hookean material behavior was utilized for the fabric skirt (μ_1=0.96 MPa, α1=-56.5, μ_2=3.57 MPa, α2=1.87, and D1=0.027 MPa). The balloon geometry in the inflated state was photographed, and the external shape profile was subsequently modeled in Rhinoceros. A simulation was conducted to replicate the balloon folding as previously described by our group [17].

Simulations of the TAVI procedure were performed with the Abaqus/Explicit solver, using the general contact approach with frictionless properties (refer to Figure 2). The S3 stent frame is initially crimped while a mock punching component displaces the native valve leaflets and calcification, creating sufficient room for the placement of the crimped device (Figure 2B and C). The deployment is simulated by inflating the balloon via the fluid-cavity method to achieve the device nominal diameter (Figures D and E). After deployment, an elastic recoil facilitated the deflation of the balloon. Frictionless contact conditions were established during deployment, whilst calcifications were incorporated into the native valve

leaflets. A Python script was created to extrapolate node coordinates and estimate the diameters associated to S3.

2.5 Statistics

To evaluate the agreement of the implanted device configuration in both in-vitro and in-silico approaches against actual post-TAVI imaging data, the device diameters were analyzed using a rigorous statistical methodology . The concordance correlation coefficient (CCC) was utilized to assess the degree of agreement between measurements. This was established by presenting the regression coefficient and beta values derived from Spearman regression. The coefficient of variation (CoV) allowed the quantification of diameter variability in relation to the mean value for each approach. The intraclass correlation coefficient (ICC) was employed to assess the reliability and consistency of repeated measurements and various methodologies. This involved estimating the ICC Indiv for repeated measurements of each method and the ICC Loneway for assessing agreement among several methods. Bland-Altman plots were generated to visually assess the agreement between in-vitro and in-silico methodologies and CT-based diameter measurements.

3. Results

The diameters of the devices were accurately measured using post-TAVI imaging, 3D printing, and in-silico modeling, and these measurements were presented together with patient demographics and calcium volume (see Table 1). No statistical association was established between device diameter and age, not with calcium volume.

3.1 FEA predictions

Figure 3 presents a comparison between numerical predictions of deformed device geometries and post-TAVI CT imaging. The blue structures showed the segmentation of the metallic stent frame derived from post-TAVI CT imaging analysis, whilst the red lines represented the deformed geometries obtained at the end of numerical simulations. A favorable correlation was qualitatively noted between the predicted deformed morphologies and the actual post-TAVI CT scans of patients following the TAVI treatment. The expansion at the annulus appeared to more accurately reflect the post-TAVI CT imaging compared to the distal segment of the implanted device. There are variations between simulation and post-TAVI CT imaging with respect to the implantation depth. These are probably caused by metallic artifacts or different operators from in-vivo to in-vitro.

3.2 3D printing

Following CT imaging of 3D printed replicas, multiplanar reformatting was utilized to assess the implantation quality perpendicular to the aortic valve at the aortic valve annulus level (Figure 4). Multiplanar reformatting refers to the process of reconstructing images in planes other than the standard axial plane from the volumetric data acquired during the CT imaging. In CT imaging, the implanted stents exhibited brilliant structures, demonstrating excellent conformability to the flexible phantom as shown by Figure 5. Only a few instances revealed discrepancies between the stent frame and the phantom wall, likely occurring near the aortic commissures. The stent frame assumed a nearly round or elliptical shape based on the anatomical features of the aortic root and the patterns of calcification.

3.3 Device diameter agreement

Table 2 illustrates the correlation and concordance of post-TAVI CT-derived diameter measurements with those obtained from both 3D printing and simulations. The low correlation and beta coefficients between CT and 3D printing show a poor association and limited linear relationship among the methods (Figure 6A). Furthermore, the low concordance and interclass correlation coefficients indicate a lack of agreement between CT-based diameter measurements and those derived from the scanned 3D printed phantom. In terms of diameter measurement variability, both in-silico and 3D printing exhibited greater coefficient of variation values compared to post-TAVI CT diameter estimates. This suggests that certain approaches may possess method-specific nuances. The reliability of in-silico predictions demonstrated strong consistency with post-CT diameter estimations (ICC Individual of 0.614) and superior agreement across methodologies (ICC Loneway of 0.628). Numerical estimates exhibited significant variability, with a coefficient of variation of 8.991, indicating increased dispersion compared to the mean. The correlation and beta coefficients between post-TAVI CT and simulations were moderate (Figure 5C).

Figures 6B and 6D present Bland-Altman graphs that quantify the biases in post-TAVI CT-derived diameter assessments using both 3D printing and finite element analysis (FEA) modeling. The diameter measurements from post-TAVI imaging exhibited a bias of ±1.1 units when compared to 3D printed replicas (with limits of agreement spanning from -4.14 to 1.92) and a bias of 0.29 units in relation to finite element analyses (with limits of agreement ranging from -3.44 to 3.38).

4. Discussion

The current study conducted a robust statistical assessment of the agreement of S3 medical device conformability to the human host against in-vitro and in-silico techniques,

taking advantage of ad hoc post-TAVI CT imaging data from TAVI patients. A statistical evaluation was carried out using various quantitative metrics and plots to determine variability and consistency among methodologies. The most notable observation is that numerical predictions demonstrate greater concordance with post-TAVI CT-derived diameter measures; however, neither approach attains an exact correspondence with reference imaging. The discrepancies may be attributed to computational modeling assumptions or boundary conditions; nevertheless, the uncertainty and intra-observer variability of post-TAVI CT diameter measurements must also be taken into account as potential explanations. This study offers significant insights into the establishment of a comprehensive validation framework for the credibility assessment of medical devices for TAVI.

4.1 The need for FEA validation of TAVI

The structural simulation of TAVI has generated significant interest within the scientific community as a pre-operative tool for determining optimal device placement and predicting possible complications. This is exemplified by innovative biotechnology such as Feops and Dasi simulation, which offer services to clinicians seeking to predict the biomechanical responses of TAVI-related devices to human hosts. These methods are gaining popularity in the clinical field so that in-silico is currently being investigated for other structural cardiac interventions (such as left atrial appendage closure) and vascular therapies [19]. Nevertheless, the credibility of such computational tools has been established through the acceptance of clinically observable data rather than rigorous study of the proposed biomedical predictive software during the design phase. This is likely attributable to the recommendation against post-TAVI CT imaging in TAVI patients due to their age and the risk of renal impairment associated with contrast agent administration. Utilizing post-TAVI

imaging data, the patient-specific TAVI model exhibited good repeatability (ICC Indiv = 0.614) and considerable concordance (ICC Loneway = 0.628) in predicting S3-related diameters compared to actual post-TAVI CT data. It should be noted that the post-TAVI scans utilized for comparison were obtained 30 days following the procedure, allowing for potential vascular remodeling or tissue adaption to occur. This may restrict the accuracy of direct anatomical comparisons with earlier in-silico models. Although the material models contribute to disparities in agreement, we have previously shown that post-TAVI CT imaging possesses an intrinsic inaccuracy of 5% in the real device diameter due to the occurrence of metallic artifacts [13]. Intra-observer variability in diameter measurements provides an additional source of uncertainty, resulting in variations and unexpected discrepancies in the concordance between the two approaches. In general, numerical predictions are accurate and methodologically coherent with post-TAVI imaging. Our computational model can benefit from a deep uncertainty quantification and sensitivity analysis to improve model credibility. An ongoing study based on the cumulative distribution function demonstrated a high predictive accuracy of the present patient-specific TAVI model, with errors between simulation and actual patient clinical data lower than 10% in twenty patients. Clinical data for validation comprised the S3 device diameter expansion in the human host as gathered by post-TAVI imaging. Sensitivity analysis revealed that the most influential model parameters were the balloon expansion.

4.2 Reliability of 3D printing

Consistent with the current study, Zhao and colleagues [20] developed both in-vitro and in-silico methodologies to evaluate the mechanical performance of TAVI devices manufactured using additive manufacturing. The stent frame of the S3 device was produced using laser powder bed fusion technology and then utilized in flexible, patient-specific phantoms as presented here. At the same time, FEAs were performed to replicate

the same deployment strategy and then compared with CT-based reconstructed geometries of phantom models. The 3D-printed S3 structure displayed fractures around stress concentrations, with the relative error in diameter between in-silico and in-vitro measurements determined at seven device heights, ranging from 1.01% to 3.17%. The agreement was limited to two patient models using fused and non-fused native valve leaflets. Likewise, Anam et al. [21] undertook an in-vitro validation of the numerical model utilizing 3D printed replicas and X-ray imaging for the self-expandable Evolut R device. This work is, to our knowledge, the first comparison of 3D printed TAVI replicas with actual CT imaging data. A low concordance correlation coefficient and poor Pearson's correlation indicate that the 3D printing process generates inconsistencies, hence diminishing its prediction accuracy for device sizing. These discrepancies presumably arise from the inherent limits of our 3D printing method, such inconsistencies in layer deposition or resin contraction during curing. The justification for the proposed 3D printing method is based on the utilization of a non-linear, elastomeric rubberlike resin, which has been employed in analogous studies due to its elongation characteristics that align with those documented in literature for the aortic root of elderly individuals [21]. The calibration of the biomechanical response of 3D printed phantoms has been suggested by decreasing the wall thickness to achieve a more compliant phantom. Our 3D printed model can also benefit from the incorporation of stiff calcific plaques by overmolding process during fabrication.

5. Conclusion

This study was undertaken to assess the predictive capabilities of patient-specific computational simulation and 3D-printed models by a rigorous comparative analysis against actual post-TAVI imaging. While FEA demonstrated superior agreement with post-TAVI imaging, neither method achieved perfect concordance, indicating the need for further refinement of these engineering technologies. The findings emphasize the

importance of validating predictive tools for TAVI planning to enhance clinical accuracy and patient outcomes. Future research should focus on standardizing numerical simulations and refining material and process for developing 3D-printed replica. Advancing these methodologies will support the development of more reliable patient-specific planning tools for next-generation transcatheter heart valves and unexpected device underperformance.

Ethics approval and consent to participate

This study was approved by the IRCCS ISMETT Ethics Committee (approval no. IRRB04/04). All participants provided written informed consent prior to enrolment in the study.

Consent for publication

All authors were fully involved in the study and preparation of the manuscript which contribution originality can be confirmed by members of ISMETT and the University of Palermo. All authors approve the submission.

Availability of data and material

The datasets generated during and/or analyzed during the current study are not publicly available due to ethical issues but are available from the corresponding author on reasonable request.

Competing interests

The authors declare that they have no known competing financial interests or personal relationships that could have appeared to influence the work reported in this paper.

Funding

Granted by European Commission – Next Generation EU – PNRR M6 – C2 – Investimento 1.3: Sviluppo di tecnologie e percorsi innovativi per la salute – Iniziativa PNC0000003 dal titolo “ANTHEM: AdvaNced Technologies for Human-centrEd Medicine” – CUP B53C22006700001.

Reference

1. Nkomo VT, Gardin JM, Skelton TN, Gottdiener JS, Scott CG, Enriquez-Sarano M. Burden of valvular heart diseases: a population-based study. Lancet. 2006;368(9540):1005-11. doi: 10.1016/S0140-6736(06)69208-8.

2. Attinger-Toller A, Ferrari E, Tueller D, Templin C, Muller O, Nietlispach F, Toggweiler S, Noble S, Roffi M, Jeger R, Huber C, Carrel T, Pilgrim T, Wenaweser P, Togni M, Cook S, Heg D, Windecker S, Goy JJ, Stortecky S. Age-Related Outcomes After Transcatheter Aortic Valve Replacement. Jacc-Cardiovasc Inte. 2021;14(9):952-60. doi: 10.1016/j.jcin.2021.01.042.

3. Leon MB, Smith CR, Mack M, Miller DC, Moses JW, Svensson LG, Tuzcu EM, Webb JG, Fontana GP, Makkar RR, Brown DL, Block PC, Guyton RA, Pichard AD, Bavaria JE, Herrmann HC, Douglas PS, Petersen JL, Akin JJ, Anderson WN, Wang D, Pocock S, Investigators PT. Transcatheter aortic-valve implantation for aortic stenosis in patients who cannot undergo surgery. N Engl J Med. 2010;363(17):1597-607. doi: 10.1056/NEJMoa1008232.

4. Levin D, Mackensen GB, Reisman M, McCabe JM, Dvir D, Ripley B. 3D Printing Applications for Transcatheter Aortic Valve Replacement. Current cardiology reports. 2020;22(4):23. doi: 10.1007/s11886-020-1276-8.

5. Brouwer J, Gheorghe L, Nijenhuis VJ, Ten Berg JM, Rensing B, van der Heyden JAS, Swaans MJ. Insight on patient specific computer modeling of transcatheter aortic valve implantation in patients with bicuspid aortic valve disease. Catheter Cardiovasc Interv. 2018. doi: 10.1002/ccd.27990.

6. Alkhouli M, Sengupta PP. 3-Dimensional-Printed Models for TAVR Planning: Why Guess When You Can See? JACC Cardiovascular imaging. 2017;10(7):732-4. doi: 10.1016/j.jcmg.2017.05.002.

7. Schmauss D, Schmitz C, Bigdeli AK, Weber S, Gerber N, Beiras-Fernandez A, Schwarz F, Becker C, Kupatt C, Sodian R. Three-dimensional printing of models for preoperative planning and simulation of transcatheter valve replacement. Ann Thorac Surg. 2012;93(2):e31-3. doi: 10.1016/j.athoracsur.2011.09.031.

8. Fujita B, Kütting M, Seiffert M, Scholtz S, Egron S, Prashovikj E, Börgermann J, Schäfer T, Scholtz W, Preuss R, Gummert J, Steinseifer U, Ensminger SM. Calcium distribution patterns of the aortic valve as a risk factor for the need of permanent pacemaker implantation after transcatheter aortic valve implantation. Eur Heart J-Card Img. 2016;17(12):1385-93. doi: 10.1093/ehjci/jev343.

9. Sturla F, Ronzoni M, Vitali M, Dimasi A, Vismara R, Preston-Maher G, Burriesci G, Votta E, Redaelli A. Impact of different aortic valve calcification patterns on the outcome of transcatheter aortic valve implantation: A finite element study. J Biomech. 2016;49(12):2520-30. doi: 10.1016/j.jbiomech.2016.03.036.

10. Brouwer J, Nijenhuis VJ, Gheorghe L, ten Berg JM, Rensing BJWM, Timmers L, Swaans MJ. The Accuracy of Patient-Specific Computer Modelling in Predicting Device Size and Paravalvular Aortic Regurgitation in Complex Transcatheter Aortic Valve Replacement Procedures. Struct Heart. 2020;4(4):320-8. doi: 10.1080/24748706.2020.1765442.

11. Finotello A, Morganti S, Auricchio F. Finite element analysis of TAVI: Impact of native aortic root computational modeling strategies on simulation outcomes. Medical Engineering & Physics. 2017;47:2-12. doi: 10.1016/j.medengphy.2017.06.045.

12. Schultz C, Rodriguez-Olivares R, Bosmans J, Lefevre T, De Santis G, Bruining N, Collas V, Dezutter T, Bosmans B, Rahhab Z, El Faquir N, Watanabe Y, Segers P, Verhegghe B, Chevalier B, van Mieghem N, De Beule M, Mortier P, de Jaegere P. Patient-specific image-based computer simulation for theprediction of valve morphology and calcium displacement after TAVI with the Medtronic CoreValve and

the Edwards SAPIEN valve. EuroIntervention : journal of EuroPCR in collaboration with the Working Group on Interventional Cardiology of the European Society of Cardiology. 2016;11(9):1044-52. doi: 10.4244/EIJV11I9A212.

13. Scuoppo R, Cannata S, Gandolfo C, Bellavia D, Pasta S. On the accuracy of the segmentation process and transcatheter heart valve dimensions in TAVI patients. Journal of Biomechanics. 2024;176. doi: ARTN 112357

10.1016/j.jbiomech.2024.112357.

14. Catalano C, Turgut T, Zhalka O, Götzen N, Cannata S, Gentile G, Agnese V, Gandolfo C, Pasta S. Establishing In-silico Credibility of Patient-Specific Finite-Element Model in a Virtual Cohort. L N Comput Vis Biome. 2024;39:311-8. doi: 10.1007/978-3-031-55315-8_34.

15. Catalano C, Scuoppo R, Turgut T, Götzen N, Cannata S, Gentile G, Gandolfo C, Pasta S. Credibility Assessment of Patient-Specific Modeling in Transcatheter Aortic Valve Implantation – Part 1: Population-Based Validation. International journal for numerical methods in biomedical engineering. 2025;inpress.

16. Scuoppo R, Catalano C, Turgut T, Götzen N, Cannata S, Gentile G, Gandolfo C, Pasta S. Credibility Assessment of Patient-Specific Modeling in Transcatheter Aortic Valve Implantation – Part 2: Uncertainty Quantification and Sensitivity Analysis. International journal for numerical methods in biomedical engineering. 2025;inpress.

17. Catalano C, Turgut T, Zahalka O, Gotzen N, Cannata S, Gentile G, Agnese V, Gandolfo C, Pasta S. On the Material Constitutive Behavior of the Aortic Root in Patients with Transcatheter Aortic Valve Implantation. Cardiovasc Eng Technol. 2024;15(1):95-109. doi: 10.1007/s13239-023-00699-7.

18. Bosi GM, Capelli C, Cheang MH, Delahunty N, Mullen M, Taylor AM, Schievano S. Population-specific material properties of the implantation site for transcatheter aortic

valve replacement finite element simulations. Journal of biomechanics. 2018;71:236-44.

19. Cruz Gonzalez I, Antunez Muinos PJ, Lopez Tejero S, Nunez Garcia JC, Rodriguez Collado J, Martin Moreiras J, Diego Nieto A, Herrero Garibi J, Diaz Pelaez E, Sanchez Fernandez PL. Left Atrial Appendage Occlusion Using the Novel Amplatzer Steerable Delivery Sheath Combine With FEops HEARTguide. JACC Cardiovascular interventions. 2021;14(21):e301-e4. doi: 10.1016/j.jcin.2021.08.055.
20. Zhao X, Eren OC, Molyneux A, Geekie L, Curzen N, Bressloff NW. Development of a methodology for in vitro and in silico simulation of transcatheter aortic valve replacement using 3D-printed valve frames. Computers in biology and medicine. 2025;186:109690. doi: 10.1016/j.compbiomed.2025.109690.
21. Anam SB, Kovarovic BJ, Ghosh RP, Bianchi M, Hamdan A, Haj-Ali R, Bluestein D. Validating In Silico and In Vitro Patient-Specific Structural and Flow Models with Transcatheter Bicuspid Aortic Valve Replacement Procedure. Cardiovasc Eng Technol. 2022;13(6):840-56. doi: 10.1007/s13239-022-00620-8.

Figure Legend

Figure 1: Pictures showing the (A) 3D printed replica of patient aortic root just after the manufacturing and post-processing and (B) balloon system and S3 device stent frame as provided by manufacturer.

Figure 2: Simulation steps of TAVI simulation starting from (A) the reference configuration with the patient-specific model and the assembly with the delivery system, (B) the crimped device and folded balloon prior the deployment, (C) half and (D) full balloon inflation, and (E) final deformed shape of implanted device with the anatomic level for device diameter measurement

Figure 3: Longitudinal and cross-sectional views of patient-specific TAVI model showing the simulated shape of S3 device (red color) and actual CT shape after TAVI procedure (blue color)

Figure 4: Photography of 3D-printed replica with the in-vitro deployment of S3 device

Figure 5: CT imaging od 3D-printed replica showing the metallic stent frame at aortic valve annulus

Figure 6: Regression curves and Blant-Altman plots showing the comparison of diameter measurements between 3D printing (3Dp) and post-TAVI CT imaging (top row) and between FEA and post-TAVI CT imaging (bottom row)

Table 1: Comparison of aortic outflow tract diameters measured using three methodologies: CT imaging, 3D printing models, and in-silico predictions.

				CT Imaging			3D printed			FEA		
	Age (yrs)	S3 size (mm)	Calcification Volume (mm^3)	Inflow (mm)	Midflow (mm)	Outflow (mm)	Inflow (mm)	Midflow (mm)	Outflow (mm)	Inflow (mm)	Midflow (mm)	Outflow (mm)
#1	82	26	93.6	24.0	24.0	23.5	21.6	22.8	22.1	23.3	24.6	26.3
#2	83	23	93.0	21.5	21.1	22.9	21.9	21.7	22.7	22.6	20.2	23.2
#3	84	23	96.5	22.6	22.1	23.7	22.6	21.6	22.1	22.0	20.2	23.4
#4	78	26	89.5	24.3	23.6	25.3	23.8	23.9	25.4	25.5	24.3	26.4
#5	77	23	92.6	22.4	22.1	23.5	20.9	21.7	21.1	22.5	20.3	23.3
#6	80	23	91.6	20.9	22.9	23.9	22.3	21.7	18.9	21.9	19.5	23.5
#7	93	23	91.1	22.4	22.1	23.5	21.3	20.1	20.3	22.6	19.9	23.0
#8	81	23	91.0	21.6	22.1	23.5	23.5	21.9	20.8	24.5	24.6	26.5
#9	79	26	92.4	22.7	22.6	23.8	22.2	21.8	21.7	23.0	21.5	24.3
#10	57	23	93.2	24.6	23.4	25.1	21.9	20.7	21.9	22.6	20.2	23.5

Table 2: Agreement on the diameter measurements at different levels of S3 device .

	R	Beta	Beta SE	CCC	CV	ICC Indiv	ICC Loneway
CT vs 3D printing	0.224	0.196	0.224	0.165	6.065	0.363	0.092
CT vs FEA	0.518	0.291	0.518	0.479	8.991	0.614	0.628

Note: R2 = coefficient of correlation; Beta = regression coefficient; Beta SE = standard error of the regression coefficient; CCC = coefficient of concordance; CV = coefficient of variation for 3Dp or FEA (CV_{CT}=5.041); ICC Indiv= interclass correlation coefficient for individual measurements; ICC Loneway= interclass correlation coefficient for One-way random effects

Figure 1

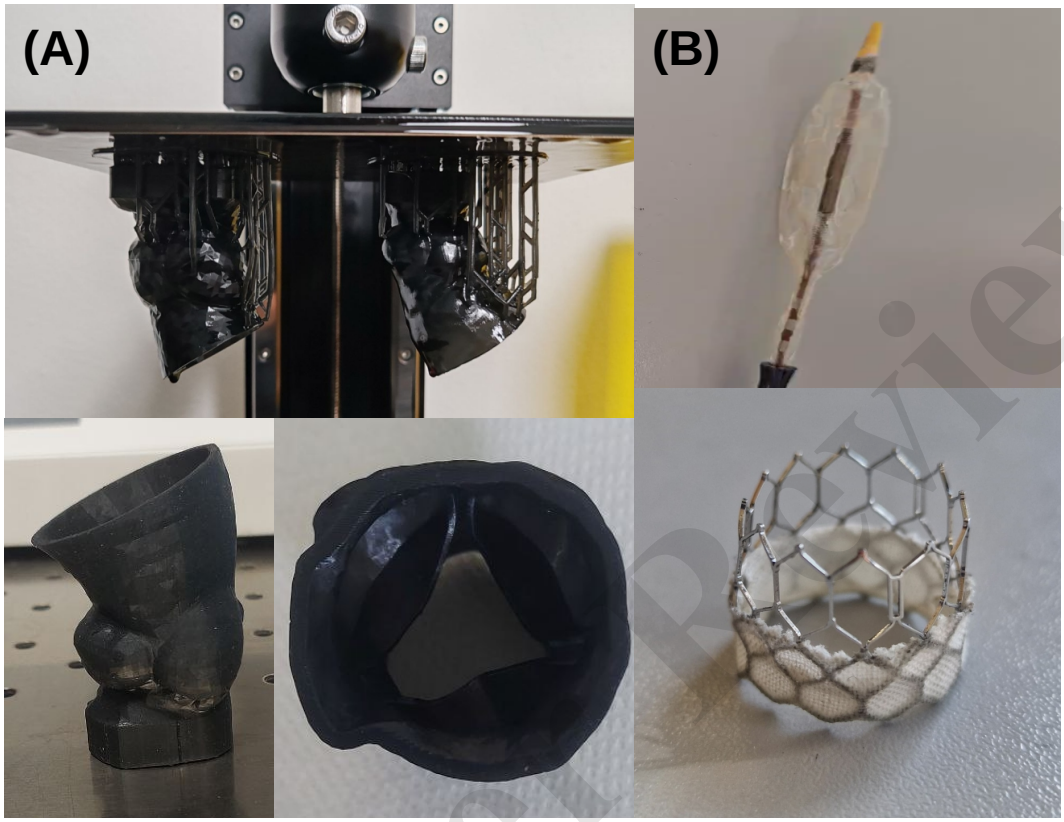

Figure 2

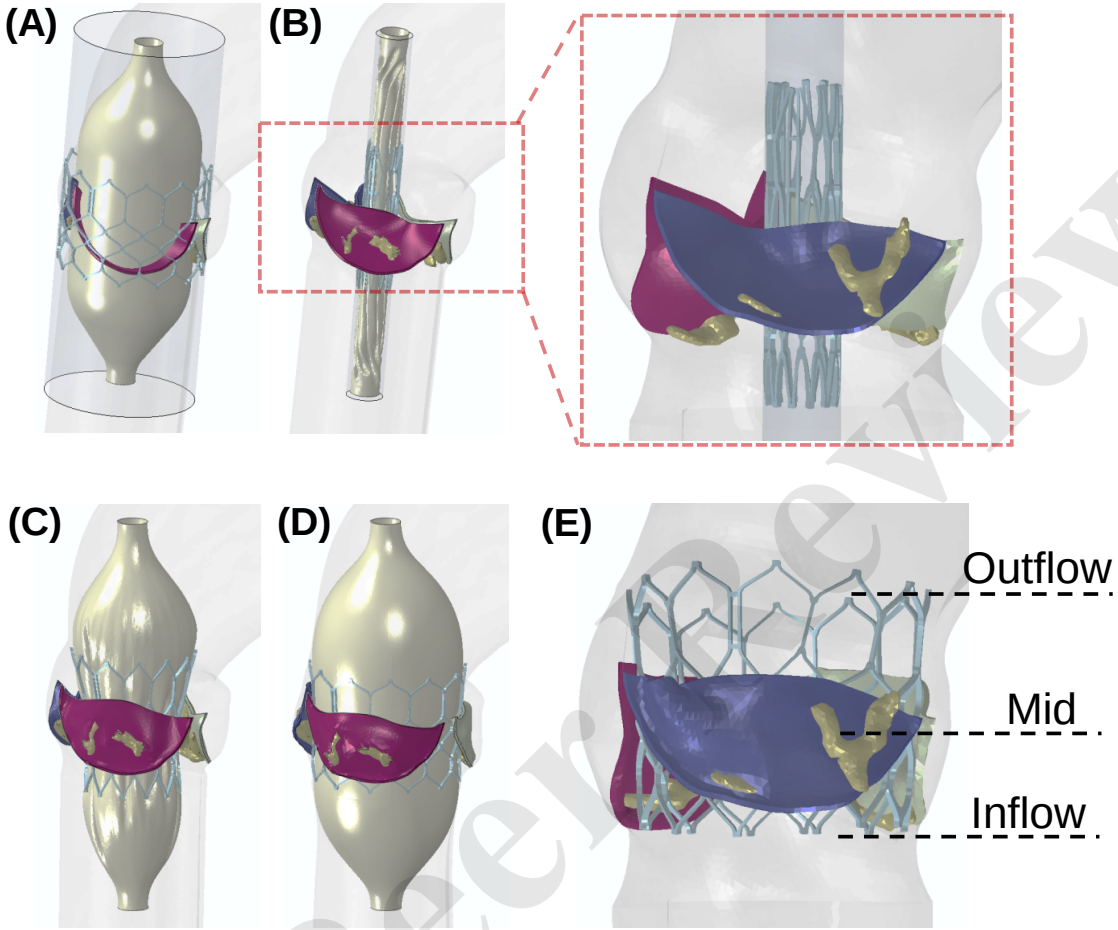

Figure 3

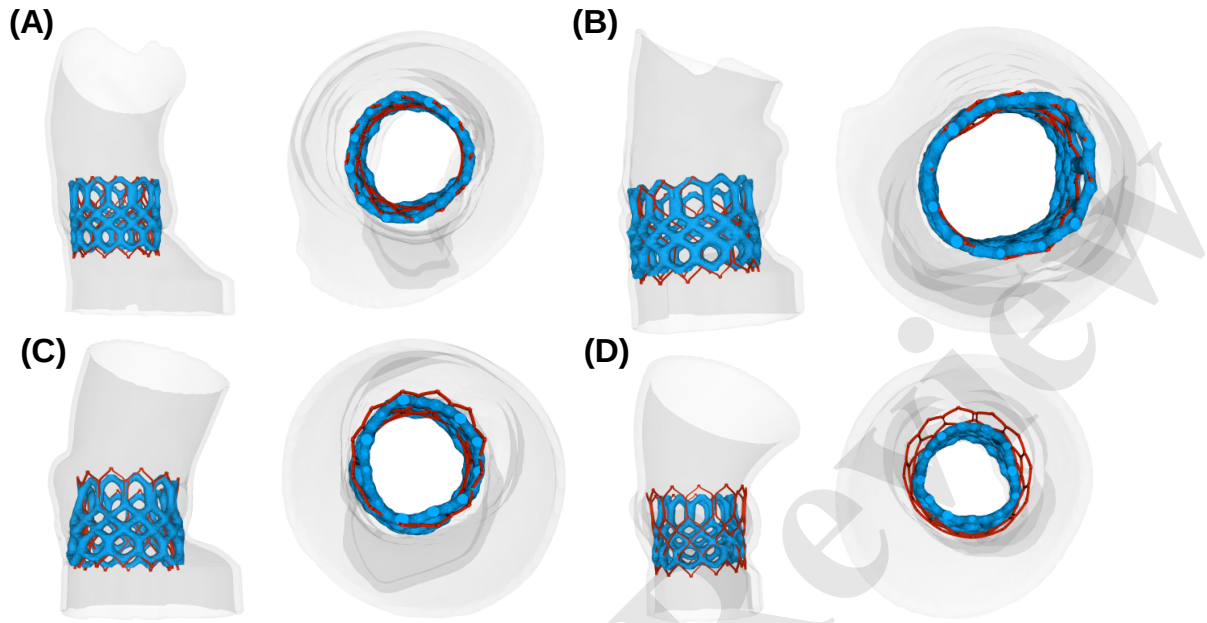

Figure 4

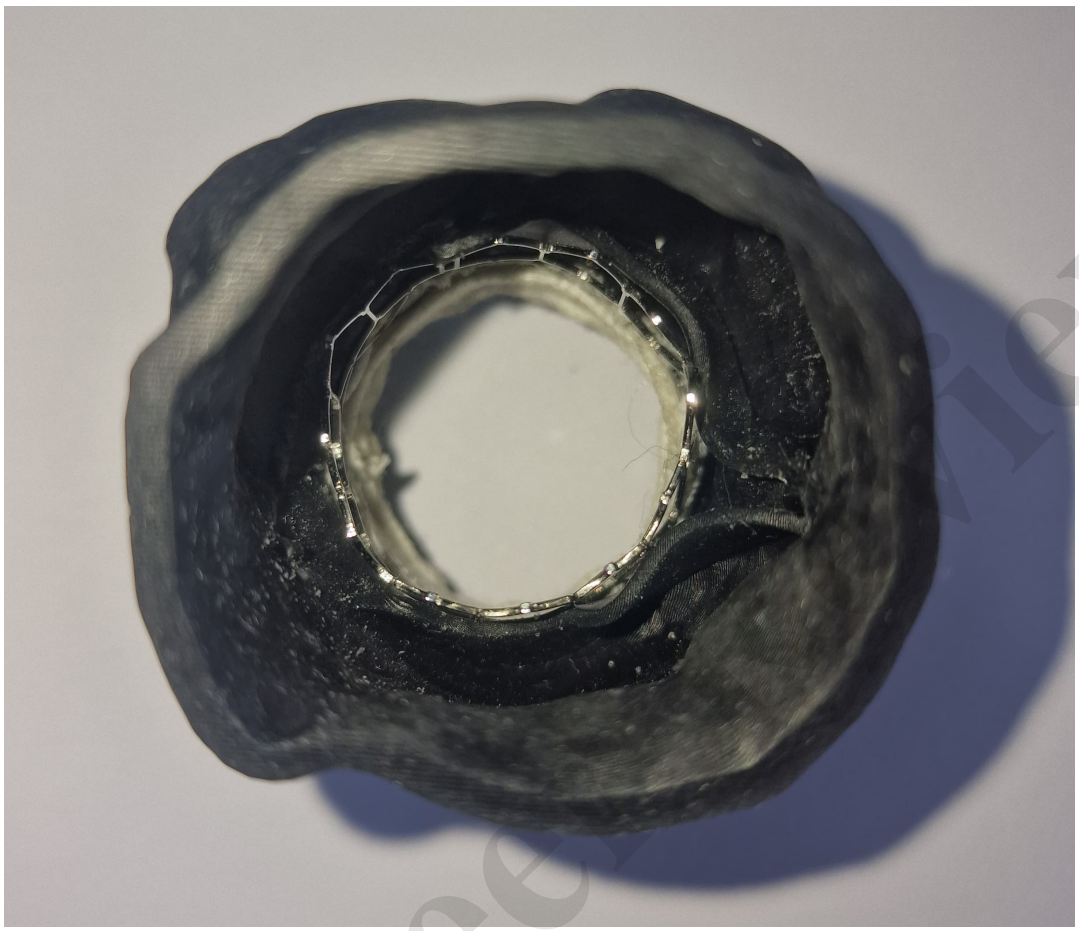

Figure 5

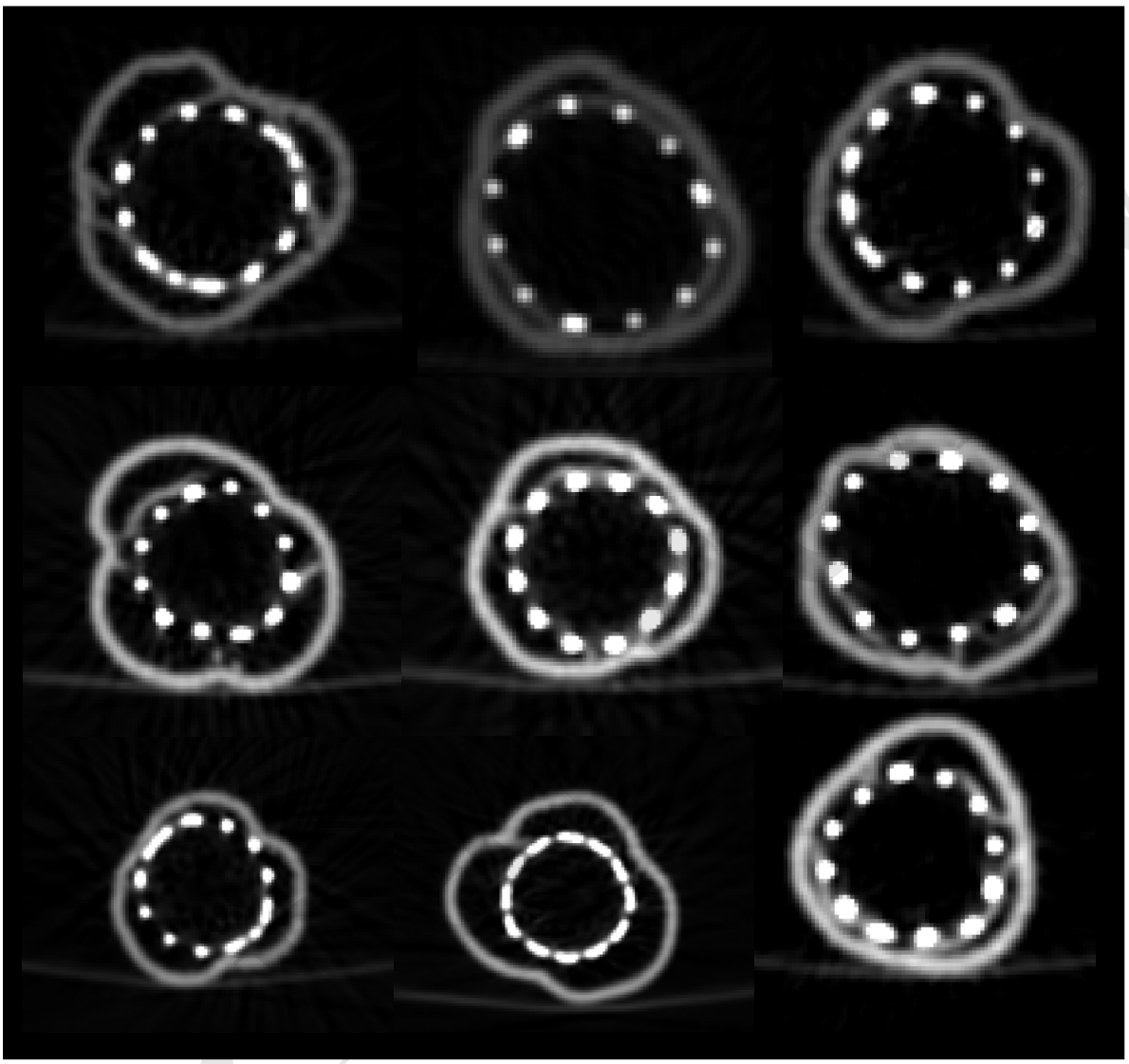

Figure 6

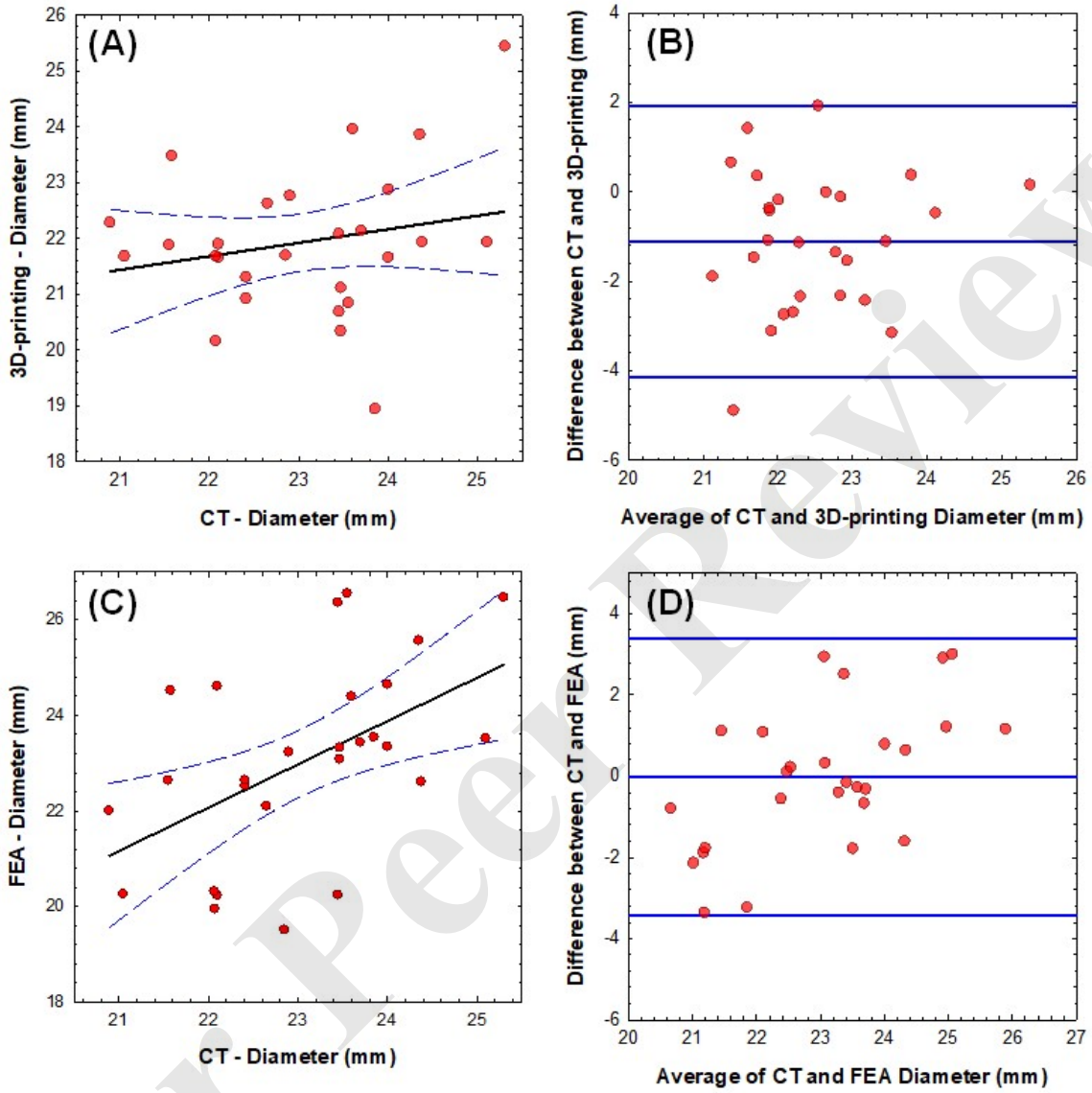

Reviewer #2

We would like to express our gratitude to the reviewer for providing valuable and constructive comments that have undoubtedly contributed to the enhancement of our manuscript. We have thoroughly considered these comments while preparing the revised version of the paper and are confident that it addresses all the critiques raised. All modifications made to the document have been highlighted in yellow to distinguish them from the previous version.

GENERAL COMMENTS

1. The sentence "Following the optimization of parameter settings, the aortic wall and valve leaflets were manufactured with thicknesses of 2 mm and 0.5 mm, respectively" is unclear. It would be helpful to clarify which specific parameters were optimized and how this optimization influenced the decision to use these particular thickness values. Were these thicknesses a result of the optimization, or were they fixed inputs?.

Reply: we thank the reviewer to point out this aspect of 3D printing. Indeed, we performed several test to optimize the 3D printing parameter setting and thus obtain the expected thickness value for the phantom model (ie, 2 mm for the aorta and 0.5 mm for the valve leaflets). The printing of the aortic wall was not influenced by printing parameter as the 2 mm value is widely reported in literature. Differently, we had to print the valve leaflets with a thickness slightly higher than that reported in literature (0.3 – 0.4 mm) to avoid failure of the whole phantom model printing. The text was rewritten with the following:

“Optimization of parameter settings was required to fabricate the thin structure of valve leaflets. Specifically, layer height, exposure and thickness were varied to achieve a successful printing of valve leaflets without layer delamination or defects. The optimal key printing parameters comprised a layer height of 50 μm, a bottom layer count of 5, a speed of 60 mm/min, and an exposure duration of 10 seconds per layer to obtain optimal polymerization. Ten transition layer counts were employed to improve interlayer adhesion, with a rest period of 2 seconds established before and after lifting and retracting. Material support was restricted to the aorta wall and not utilized for the valve leaflets due to the risk of lacerating the delicate surface leaflets. The resulting thickness was 2 mm for the aortic wall and 0.5 mm for the valve leaflets.”

2. Material properties are provided for calcium, but not for the other materials used. For completeness and reproducibility, it is recommended to include the mechanical properties of all materials mentioned, either in the main text or in a summary table.

Reply: the material properties for the aortic wall, native valve leaflets and skirt were added with the following sentences:

"The resulting neo-Hookean material parameters were in the range of 0.25- 1.24 MPa for the aortic wall and 0.68-2.5 MPa for the valve leaflets"

and

"A second-order Ogden model was employed for the biological valve leaflets, while a neo-Hookean material behavior was utilized for the fabric skirt (m_1=0.96 MPa, a1=-56.5, m_2=3.57 MPa, a2=1.87, and D1=0.027 MPa)"

The material properties of stent frame are properly cited as were collected from literature data so that we prefer not to add if permitted by the reviewer.

3. There appears to be a typographical error—specifically, two dots—at the end of paragraph 3.2.

Reply: fixed

4. When referring to "multiplanar reformatting," please consider adding a citation or brief explanation for readers who may not be familiar with the technique.

Reply: the following sentence was added to clarify the meaning of multiplanar reformatting:

"Multiplanar reformatting refers to the process of reconstructing images in planes other than the standard axial plane from the volumetric data acquired during the CT imaging"

Reviewer #2

We would like to express our gratitude to the reviewer for providing valuable and constructive comments that have undoubtedly contributed to the enhancement of our manuscript. We have thoroughly considered these comments while preparing the revised version of the paper and are confident that it addresses all the critiques raised. All modifications made to the document have been highlighted in yellow to distinguish them from the previous version.

GENERAL COMMENTS

1. Lack of Uncertainty Quantification: A major concern is the absence of uncertainty quantification. When proposing a computational model for predictive use, especially in a clinical context, uncertainty analysis is essential to establish credibility and reliability. The conclusions regarding the superiority of FEA are currently too general and not sufficiently supported by a rigorous quantitative framework. The authors are encouraged to include a comprehensive uncertainty quantification and sensitivity analysis.

Reply: We agree with the Reviewer that the credibility of the computational model will increase if an uncertainty quantification and sensitivity analysis is shown. This was indeed the target of a different publication under consideration in a different journal that we prefer to report here but not in the paper as the central message of the present paper is different. In brief, we have performed a uncertainty quantification and sensitivity analysis on the material parameters, aortic wall thickness, boundary conditions and procedural parameters of the patient-specific TAVI model. For structural TAVI simulation, the error between the simulation and actual clinical parameters were found lower than 10% for either the 23 and 26 mm Sapien 3 device. Sensitivity analysis revealed that the balloon expansion and the elastic behavior of the device are the most influential parameters. Please find below two figures shown the results for the sensitivity analysis and uncertainty quantification. This data will be available soon in one peer-review paper and a book chapter. The following sentence was added in the Section 4.1 to highlight these aspect:

“Our computational model can benefit from a deep uncertainty quantification and sensitivity analysis to improve model credibility. An ongoing study based on the cumulative distribution function demonstrated a high predictive accuracy of the present patient-specific TAVI model, with errors between simulation and actual patient clinical data lower than 10% in twenty patients. Clinical data for validation comprised the S3 device diameter expansion in the human host as gathered by post-TAVI imaging. Sensitivity analysis revealed that the most influential model parameters were the balloon expansion.”

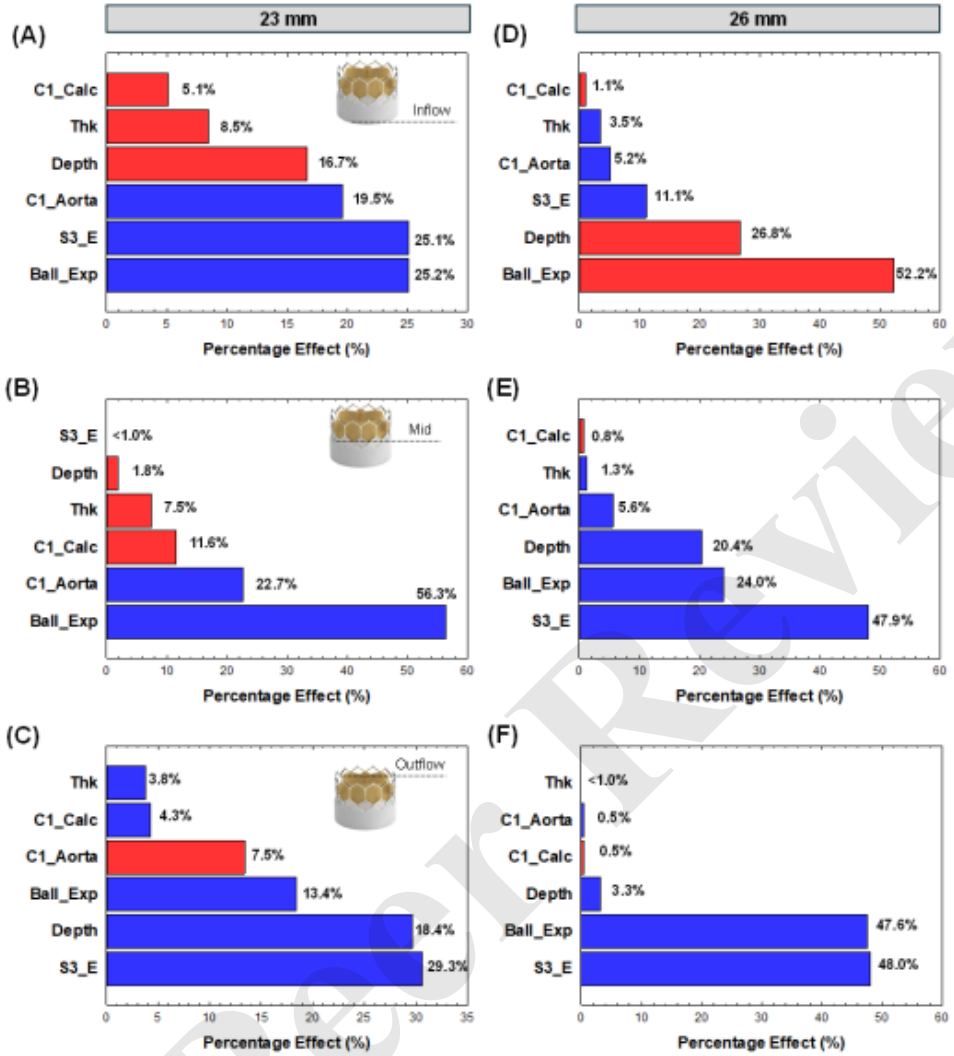

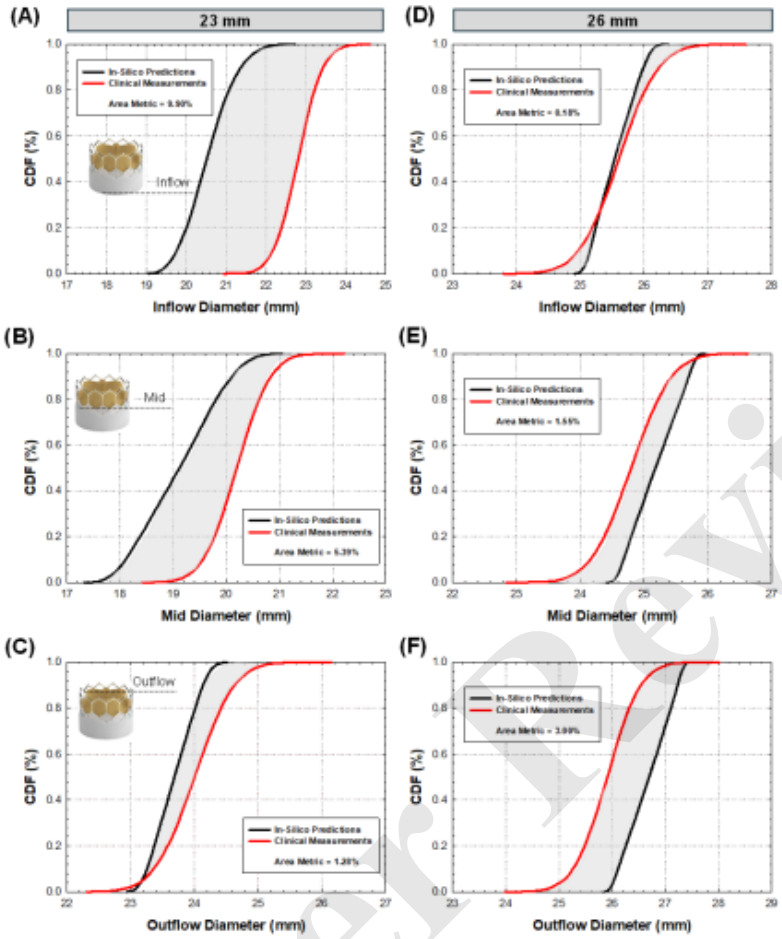

2. Validation Protocol: Comparing FEA directly with in vivo data without prior validation raises methodological concerns. A robust workflow would involve first validating the FEA model against known benchmarks or experimental data before using it to predict in vivo behavior. This sequence is essential to establish trust in the simulation results.

Reply: As described in the previous comment, the validation of the FEA model was carried out against clinical data. For validation, we used post-TAVI imaging data including the device diameter expansion in the human host at different anatomic levels (please see figure described previously). This data were compared to numerical prediction and the level of agreement was determined in a probabilistic manner by cumulative distribution function. The sentence added in Section 4.1 (as described in the previous comment) addresses this aspect while we prefer not to add specific data on the validation as a deep analysis on this is currently under consideration in a journal and a book chapter.

3. Physiological Considerations: The study does not clarify whether pre-stress of the aortic wall is accounted for in the FEA simulations. Given the significant role of residual stress and aortic biomechanics, this omission could substantially affect the validity of the comparison. Additionally, since the post-operative CT is acquired at 30 days, it is plausible that vascular remodeling or tissue adaptation may have occurred, potentially limiting the accuracy of direct anatomical comparisons with earlier models. This possibility should be discussed.

Reply: according to our previous investigation, the influence of pre-stress is low in this patient as the aortic root is remarkably stiff. Please find below an example of stress-free configuration (green color) superimposed on the diastolic shape (grey color) for the aortic wall of one patient. It can be noted that the amount of vessel contraction is minimal when using the approach developed by Krishnan et al ICVTS 2015. As the pre-stress was not indeed used in the present investigation, the following sentence was added in Section 2.4:

"The aortic wall model did not account for the pre-stress of the aortic wall, which presumably affects the TAVI simulation and wall stress distribution."

Regarding the time period from TAVI to post-operative acquisition, please consider that this is dictated by the clinical routine. In general, post-TAVI CT imaging is not necessary in this patient and may lead to renal dysfunction due to the contrast agent as the patient are quite old. We agree with the reviewer that remodeling of the aortic root may occur in the 30 days from TAVI to post-TAVI

imaging and that this may have influenced the comparison here performed. This is indeed a study limitation so that the following sentence was added in Section 4.1:

“It should be noted that the post-TAVI scans utilized for comparison were obtained 30 days following the procedure, allowing for potential vascular remodeling or tissue adaption to occur. This may restrict the accuracy of direct anatomical comparisons with earlier in-silico models.”

4. Measurement Locations and Metrics: It is unclear exactly where the diameter measurements are taken across the different models. A figure clearly illustrating the measurement points across the FEA, 3D-printed, and in vivo models is essential for transparency and reproducibility. Moreover, relying solely on diameters might not capture the full geometric complexity—area-based measurements and eccentricity indices would offer more comprehensive insight, especially in regions prone to asymmetric expansion (e.g., the annulus or LVOT).

Reply: the Figure 2 and its caption was adjusted to show the anatomic level for the measurement of device diameter. While we agree with the reviewer that other metrics exist, the device diameter was used as this is the most simple and commonly used metric by radiologist to assess the device expansion.

5. Consistency of Compared Models: The experimental setup seems to lack consistency in model components. In the 3D-printed model, the Edwards valve seems to be implanted with the skirt, whereas the FEA model does not appear to include it. This inconsistency may impact mechanical behavior and contact dynamics, leading to an unfair comparison. If the goal is to compare the predictive capacity of each modeling strategy, they should ideally be tested under equivalent conditions.

Reply: the skirt was not included in the numerical model but please consider that expansion is mainly driven by the stent frame material. The latter has significantly higher stiffness of the skirt that is merely used for reducing leakage. Nothing was added in the text if permitted by the reviewer.

6. Figures and Visual Evidence: In Figure 3, the simulated valve appears to differ in height compared to the in vivo reconstruction, which should be addressed or clarified. Additionally, Figure 4 does not provide compelling or representative results and should either be revised or replaced with a more informative visualization. The inclusion of comparisons across cross-sectional areas, eccentricity plots, and contact pressure maps would enhance the analysis.

Reply: Regarding Figure 3, please consider in general that implantation depth is in general with 1/3 of the device facing the LVOT and this was done for both in-vivo and in-silico condition. There are slight difference that may be due to several factors like different operators from in-vivo to in-vitro or metallic artifact. The following sentence was added in Section 3.1:

“There are variations between simulation and post-TAVI CT imaging with respect to the implantation depth. These are probably caused by metallic artifacts or different operators from in-vivo to in-vitro.”

Figure 4 simply shows a representative 3D printed phantom model with the implanted S3. We retain this is can be considered as a result because the study focuses on the developing 3D printed geometry and implanting the device for further comparison. We retain that the reader should be informed of the actual representation if the reviewer agrees.